Water Science and Technology: Water Supply Vol 2 No 3 pp 167–173 © IWA Publishing 2002

Numerical simulation of chlorine disinfection processes

D.J. Greene*, C.N. Haas*, and B. Farouk**

* School of Environmental Science, Engineering and Policy, Drexel University, 3141 Chestnut Street, Philadelphia, PA 19104, USA

** Department of Mechanical Engineering and Mechanics, College of Engineering, Drexel University, 3141 Chestnut Street, Philadelphia, PA 19104, USA

Abstract The efficacy of disinfection processes in water purification systems is governed by several key factors including reactor hydraulics, disinfectant chemistry and microbial inactivation kinetics. The objective of this work was to develop a computational fluid dynamics (CFD) model to predict flow structure, mass transport and chlorine decay in a continuous flow pilot scale reactor. These predictions were compared with experimental measurements for model validation. The current research demonstrates that inlet configurations can significantly impact reactor hydrodynamics.

Keywords Chlorine; computational fluid dynamics; disinfection; reactor engineering

Introduction

The efficacy of disinfection processes for potable water is governed by several key factors including reactor hydraulics, disinfectant chemistry and microbial inactivation kinetics. Computational fluid dynamics (CFD) modeling is a tool that can be utilized to integrate these key elements for optimization of disinfection reactors. Historical CFD modeling efforts have focussed primarily on investigation of reactor hydraulics, at various Reynolds numbers (Re). Re is defined as UR_H/ν, where U is the average axial reactor velocity, R_H is the hydraulic radius associated with U, and ν is the kinematic viscosity. R_H in a rectangular reactor is defined as the channel flow area divided by the wetted perimeter of the channel; both the flow area and wetted perimeter are perpendicular to U. Several researchers have evaluated full-scale chlorine contactors with a turbulent flow regime at intermediate Re (i.e. Re = 10^5–10^6) based on a R_H of 5.0–10 m and U of 0.03–0.2 m/s (Stambolieva *et al*., 1993; Crozes *et al*., 1997; Hannoun and Boulos, 1997). Modeling of low Re flows (i.e. Re = 10^3–10^4) has also been conducted for a pilot scale contactors with a R_H of 0.4 m and U of 0.005–0.02 m/s (Crozes *et al*., 1997; Wang and Falconer, 1998). The present research is concerned with hydrodynamics, mass transport and disinfectant decay in low Re flow.

The objectives of this study were to:

- simulate flow, tracer transport and chlorine decay in a pilot-scale reactor with the use of a three-dimensional (3D) CFD model;
- validate numerical model with experimental results;
- evaluate the effect of reactor inlet configurations on reactor performance (i.e. degree of dispersion).

Numerical modeling of low Re flows was performed for a pilot-scale serpentine chlorine contactor that was previously evaluated with conventional tracer analysis, as detailed by Haas *et al*. (1995).

Methods

A series of batch and continuous flow experiments were conducted by Haas *et al*. (1995) to assess the kinetics of chlorine decay and microbial inactivation for various source waters, chlorine species and microorganisms. In the present study, a numerical model was utilized

to predict flow fields and disinfectant concentrations in a pilot-scale disinfection reactor, illustrated in Figure 1. The open-tank, serpentine reactor includes an inlet chamber, three main passes (designated as pass 1, 2 and 3) and an effluent chamber. A sharp-crested weir immediately precedes the effluent chamber and controls the water level in the reactor. Flow enters the reactor at the inlet chamber through a 2.5 cm diameter pipe at the reactor floor. The inlet flow rate is 0.011 m^3/min., with a corresponding inlet velocity of 0.37 m/s. The average channel velocity based on the total cross-sectional area of Pass 1 is 0.001 m/s. Based on this average velocity and a corresponding hydraulic radius of 0.4 m, the Re in the reactor is 400 which indicates that the flow regime is predominantly laminar.

The reactor compartments are segregated by perforated baffle plates (designated as baffle 1, 2, 3 and 4). Each baffle is perforated with 50 holes of equal diameter, ranging from 0.64 cm for baffle 1 to 1.59 cm for baffles 2–4. The total combined area of the baffle 1 perforations is approximately 1% of the total plate area; the total combined area of the baffle 2–4 perforations is approximately 5% of the total plate area. The perforations create flow jets that promote mixing in the reactor, and thus are key features that influence the structure of the reactor flow field.

A computational model was constructed for Pass 1 of the reactor that encompasses the section starting at the inlet pipe up to baffle 2. The model is illustrated in Figure 2 and includes 50 "outlet pipes" that simulate the jets discharging downstream of baffle 2. This approach was adopted to enable fully developed velocity profiles at the model outlet to facilitate convergence in the numerical flow simulation.

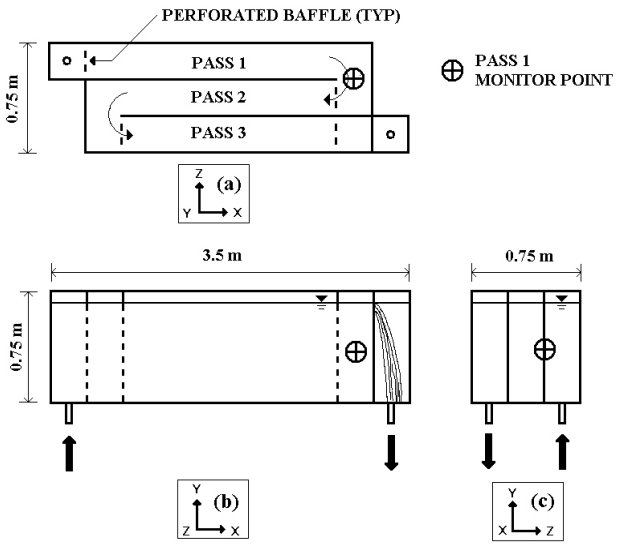

Figure 1 Pilot scale reactor configuration: (a) plan view; (b) profile view; (c) side view

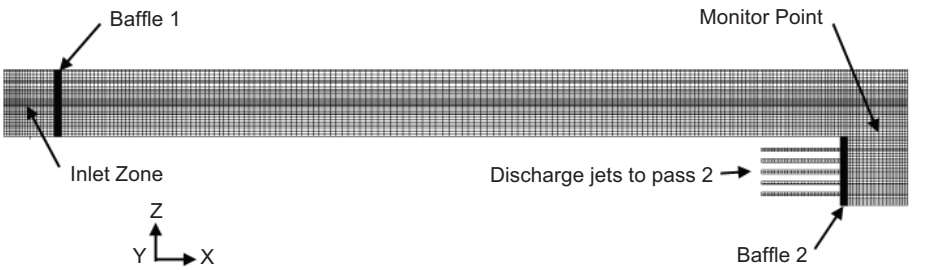

Figure 2 Computational model – Pass 1 (reactor plan view)

Governing equations

The flow field is described by the Reynolds averaged, Navier–Stokes equations for mass and momentum conservation. Although the characteristic Re of the reactor is 400, a turbulence model is required to account for localized turbulence at the pipe inlet and baffle perforations. Turbulence is characterized by an eddy viscosity model, coupled with the low Reynolds number k–ε closure model of Launder and Sharma (1974). The following equations are based on the assumptions that the flow is steady state, isothermal and incompressible.

Continuity. The continuity equation can be written as:

$$\frac{\partial \mathbf{U}_i}{\partial \mathrm{x}_i} = 0 \tag{1}$$

where $\mathbf{U}_i$ is the time averaged velocity vector.

Momentum. The momentum equation for the turbulent flow field can be written as:

$$\rho \mathbf{U}_j \left(\frac{\partial \mathbf{U}_i}{\partial x_j} \right) - (\mu + \mu_t) \frac{\partial}{\partial x_j} \left(\frac{\partial \mathbf{U}_i}{\partial x_j} + \frac{\partial \mathbf{U}_j}{\partial x_i} \right) = - \frac{\partial \left(P + \frac{2}{3} \rho k \right)}{\partial x_i} \tag{2}$$

where

$$\mu_t = C_\mu \rho \frac{k^2}{\varepsilon} \exp \left[-3.4 \left(1 + \frac{\rho \frac{k^2}{\mu \varepsilon}}{50} \right)^{-2} \right] \tag{3}$$

where P is the dynamic pressure, μ is the laminar fluid viscosity, μ_t is the turbulent fluid viscosity, k is the turbulent kinetic energy, ε is the kinetic energy dissipation rate, ρ is the fluid density, x_i is the Cartesian coordinate vector and C_μ is a model constant.

Turbulence. The distribution of the turbulent viscosity μ_t is characterized by the low Reynolds number k–ε model of Launder and Sharma (1974). The equations for k and ε can be written as:

$$\rho \mathbf{U}_i \frac{\partial k}{\partial x_i} - \left(\mu + \frac{\mu_t}{\sigma_k} \right) \frac{\partial}{\partial x_i} \left(\frac{\partial k}{\partial x_i} \right) = \mu_t \left(\frac{\partial \mathbf{U}_i}{\partial x_j} + \frac{\partial \mathbf{U}_j}{\partial x_i} \right) \frac{\partial \mathbf{U}_i}{\partial x_j} - \rho \varepsilon - 2\mu \left(\frac{\partial k^{\frac{1}{2}}}{\partial x_i} \right)^2 \tag{4}$$

$$\rho \mathbf{U}_i \frac{\partial \varepsilon}{\partial x_i} - \left(\mu + \frac{\mu_t}{\sigma_\varepsilon} \right) \frac{\partial}{\partial x_i} \left(\frac{\partial \varepsilon}{\partial x_i} \right) = C_1 \frac{\varepsilon}{k} \left(\frac{\partial \mathbf{U}_i}{\partial x_j} + \frac{\partial \mathbf{U}_j}{\partial x_i} \right) \frac{\partial \mathbf{U}_i}{\partial x_j} - C_2 f_2 \frac{\varepsilon^2}{k} - \frac{2\mu\mu_t}{\rho} \left(\frac{\partial}{\partial x_j} \left(\frac{\partial \mathbf{U}_i}{\partial x_j} \right) \right)^2 \tag{5}$$

where σ_k and σ_ε are the Schmidt numbers for k and ε, respectively. Values of the turbulence model constants C_μ, C_1, C_2 and function f_2 are prescribed by Launder and Sharma (1974); these constants were not adjusted in this study.

Mass transport and disinfectant decay. The transport and decay of a chemical species in a flow field can be described by a general convection–diffusion equation, expressed in the form:

$$\rho\frac{\partial\varphi}{\partial t}+\rho\mathbf{U}_i\frac{\partial\varphi}{\partial x_i}-\left(\rho D_\varphi+\frac{\mu_t}{\sigma_\varphi}\right)\frac{\partial^2\varphi}{\partial {x_i}^2}=S \tag{6}$$

where $S = 0$ for tracer transport and $S = -\rho k_{Cl} Cl$ for chlorine decay. φ is any scalar variable (tracer or chlorine in this study), D_φ is the molecular diffusivity of the scalar, and σ_φ is the turbulent Schmidt number of the scalar and S is the source /sink term for the scalar variable.

Boundary conditions

Dirichlet boundary conditions were specified at the inlet for the $\mathbf{U}_i$, k, ε and φ. The inlet velocity was specified only for the direction normal to the inlet face. The inlet values of k and ε are based on empirical relations (AEA Technology, 1999). The tracer is assumed to be perfectly mixed with water at the reactor pipe inlet. The outlets were designated as pressure boundaries, with Dirichlet conditions specified for pressure and Neumann conditions (i.e. zero normal gradients) specified for all other dependent variables. The boundary conditions at the solid walls of the reactor and piping represent non-slip criteria for velocity, k and ε. Zero normal flux conditions were specified for scalar variables at the walls. The free water surface of the reactor was treated as a free slip surface, with zero normal flux boundary conditions for scalar variables.

Solution procedure

The governing equations were discretized on a structured, multi-block, non-staggered grid by a finite volume technique. The computational grid was constructed for pass 1 of the reactor and consists of approximately 800,000 cells. The convective terms in the hydrodynamic Eqs (2)–(5) are discretized according to a hybrid differencing scheme prescribed by Patankar (1980). Convective terms of the mass transport/decay Eq. (6) are discretized by an upwind quadratic differencing scheme developed by Alderton and Wilkes (1988). A central difference scheme was utilized for all diffusive terms, while a fully implicit backward differencing was employed for transient terms in the dye transport simulations. The set of algebraic equations was solved by line-by-line iteration.

The hydrodynamic equations were solved using the SIMPLEC velocity-pressure coupling algorithm of Van Doormaal and Raithby (1984) to obtain the steady-state 3D flow field. Transient dye transport and steady-state chlorine decay simulations were performed by solving Eq. (6) across the "frozen" numerical flow field. Approximately 6,000 iterations were required to achieve convergence of the hydrodynamic equations, while approximately 100 iterations were required for the steady-state chlorine decay simulations. For the transient tracer test simulations, 1,200 10 s time steps were utilized; each time step is approximately 0.3% of the nominal mean residence time. Numerical simulations were performed on a PC using the general-purpose code CFX-4 (AEA Technology, 1999).

Results and discussion

Flow and mass transport

The predicted flow structure for the pass 1 inlet zone is illustrated in Figure 3. As shown, non-uniform flow jetting is predicted through the baffle 1 perforations. The significance of this flow structure is discussed in the following section. A step-feed tracer test simulation was conducted to verify the accuracy of the flow model. The simulation was performed by solving Eq. 6 (without a dye sink term) across the numerical flow field. Experimental and predicted tracer curves correlate well, as shown in Figure 4. Tracer data indicate a significant degree of fluid short-circuiting occurs since the ratio of the Pass 1 tracer effluent breakthrough time (16 minutes) to the pass 1 mean hydraulic residence time (59 minutes) is approximately 0.27.

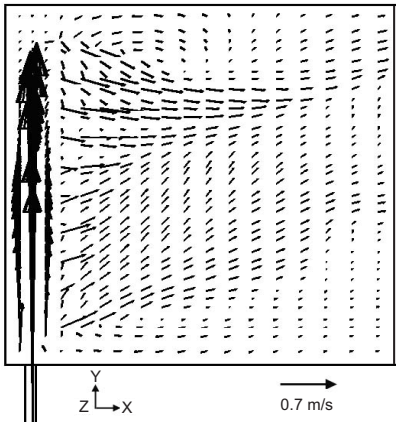

Figure 3 Predicted flow structure for reactor inlet region

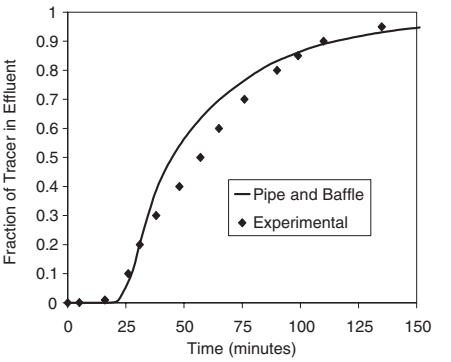

Figure 4 Predicted tracer curve for pass 1 of reactor

Reactor evaluation

Flow and tracer test simulations were performed for several alternative inlet configurations to identify the relative influence of reactor elements on the pass 1 flow structure. Specifically, the following cases were simulated:

- *Case 1*. Ideal inlet with uniform velocity profile through reactor end-wall (no inlet pipe or perforated baffle).
- *Case 2*. Same inlet condition as Case 1, with inclusion of the existing 0.64 cm perforated baffle plate (no inlet pipe).
- *Case 3*. 2.5 cm inlet pipe at reactor floor with no baffle plate.
- *Case 4*. Existing reactor, with inlet pipe and perforated baffle plate.

The predicted tracer curves for Cases 1–4 are presented in Figure 5.

Case 1 represents the ideal inlet configuration for pass 1; dispersion is caused by wall effects only. Case 2 demonstrates that the effect of the baffle plate alone on the "ideal" inlet is insignificant. In Case 3, the 0.25 cm inlet pipe causes a significant degree of dispersion since there is no baffle plate to dampen the relatively high inlet velocity at the pipe entrance. However, the surprising result is that the predicted Case 3 tracer curve exhibits

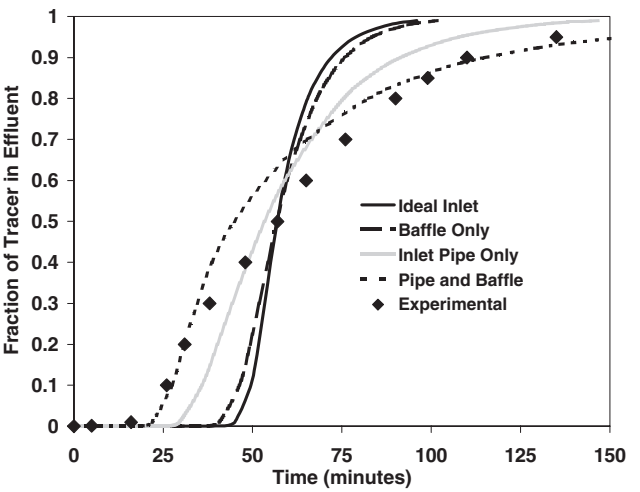

Figure 5 Predicted tracer curves for alternative inlet configurations

less dispersion than the Case 4 (existing reactor) curve. Thus, the flow model for the existing reactor predicts that the perforated baffle plate actually increases the dispersion in Pass 1, which is contrary to its intended purpose. The increased dispersion exhibited by the Case 4 tracer curve is caused by non-uniform jetting through the baffle perforations, as shown in Figure 3.

In all cases, the free liquid surface of the reactor was modeled as a flat free surface with free-slip conditions. The effect of this boundary condition in the Case 4 model is that a pressure build up is predicted in the upper region of the inlet zone. It is this pressure build up which creates the non-uniform jetting flow structure depicted in Figure 3.

The inclusion of a perforated baffle plate is not expected to significantly increase dispersion in a reactor, particularly in the case of baffle 1, where the perforations comprise approximately 1% of the reactor cross-sectional area. Modeling efforts are on-going to resolve this apparent discrepancy. Specifically, the free liquid surface will be modeled as an air–water interface (i.e. two-phase system). Although there is uncertainty with the predicted pass 1 flow structure, the pass 1 (Case 4) tracer curve fits the experimental tracer data reasonably well. More importantly, the pass 1 flow model was found to accurately predict experimental chlorine concentrations, as discussed in the following section.

Chlorine decay

A series of steady-state chlorine decay simulations were conducted by solving Eq. (6) across the Case 4 flow field, with a sink term for chlorine. The influent chlorine concentrations and decay constants (k_{Cl}) for several continuous-flow experiments were measured by Haas *et al.* (1995) and used in the simulations. Experiments were performed for varying initial doses of free chlorine and monochloramine for two different source waters. Source water A is from a reservoir and source water B is from a river. Measured decay rates in these waters ranged from 0.003–0.048 min^{-1} for free chlorine and from 0.0010–0.0015 min^{-1} for monochloramine. A representative chlorine contour plot is presented in Figure 6. Predicted and experimental chlorine concentrations at the end of reactor pass 1 are summarized in Figure 7. As shown, steady-state experimental and simulation results correlate well over a range of chlorine decay rates and doses.

Conclusions

The current research demonstrates that inlet configurations can significantly impact reactor hydrodynamics, even at very low Reynolds numbers. It is important to predict correct flow structures in a reactor when evaluating alternative configurations during the design phase. Additional modeling work is required to understand the flow structure in the existing reactor before it can be optimized. From a process viewpoint, it is critical to attain an

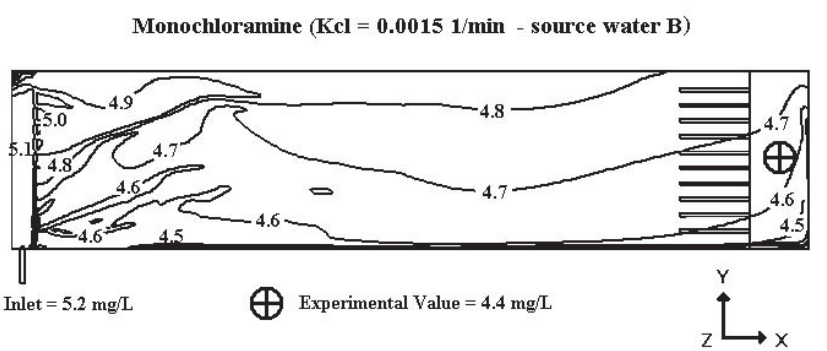

Figure 6 Predicted monochloramine concentration contour plot

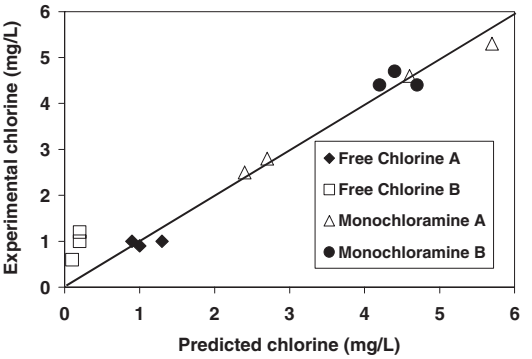

Figure 7 Predicted and experimental chlorine concentrations at end of pass 1

accurate mass transport model. The current model accomplishes this objective since both the predicted tracer curve and chlorine concentrations were in good agreement with experimental data.

Future research will involve simulation of microbial disinfection with the use of various rate laws for inactivation. Simulations will be performed for varying microorganisms, disinfectants and source waters.

Acknowledgements

The experimental work described in this paper was sponsored by the American Water Works Association Research Foundation (AWWARF) and was conducted by the Portland Water Bureau, Montgomery Watson Engineers and Drexel University. Support for the numerical modeling work was allocated from the L.D. Betz endowment at Drexel. The authors thank Mr. Mark Heath (independent consultant) for his assistance in the current modeling project.

References

AEA Technology (1999). *CFX-4.3 Solver Manual*. Oxfordshire, UK.

Alderton, J.H. and Wilkes, N.S. (1988). *Some Applications of New Finite Difference Schemes for Fluid Flow Problems*. Report No. 13234, Atomic Energy Research Establishment, Oxfordshire, UK.

Crozes, G.F., Hagstrom, J.P., Clark, M.M., Ducoste, J. and Burns, C. (1997). *Improving Clearwell Design for CT Compliance*. American Water Works Association Research Foundation Report, Denver, CO, USA.

Haas, C.N., Joffe, J., Anmangandla, U., Hornberger, J.C., Heath, M.S., Jacangelo, J. and Glicker, J. (1995). *Development and Validation of Rational Design Methods of Disinfection*. American Water Works Association Research Foundation Report, Denver, CO, USA.

Hannoun, I.A. and Boulos, P.F. (1997). Optimizing distribution storage water quality: a hydrodynamic approach. *Appl. Math. Model*, **21**, 495–502.

Launder, B.E. and Sharma, B.I. (1974). Application of the energy-dissipation model of turbulence to the calculation of flow near a spinning disk. *Letters in Heat and Mass Transfer*, **1**, 131–138.

Patankar, S.V. (1980). *Numerical Heat Transfer and Fluid Flow*. Hemisphere, Washington, DC, USA.

Stambolieva, Z., Roustan, M., Wable, O., Duguet, J.P. and Mallevialle, J. (1993). Methods for the design of chlorine contactors for drinking water treatment. *Proc. American Water Works Association Conference*. Denver, CO, USA, pp. 693–709.

Van Doormaal, J.P. and Raithby, G.D. (1984). Enhancements of the simple method for predicting incompressible fluid flows. *Numerical Heat Transfer*, **7**, 147–163.

Wang, H. and Falconer, R.A. (1998). Simulating disinfection processes in chlorine contact tanks using various turbulence models and high-order accurate difference schemes. *Wat. Res*. **5**, 1529–1543.